ELSEVIER

In situ water distribution measurements in a polymer electrolyte fuel cell

M.M. Mench*, Q.L. Dong, C.Y. Wang

*Electrochemical Engine Center, Department of Mechanical and Nuclear Engineering,
The Pennsylvania State University, University Park, PA 16802, USA*

Abstract

The overall water vapor balance and concentration distribution in the flow channels is a critical phenomenon affecting polymer electrolyte fuel cell (PEFC) performance. This paper presents, for the first time, results of a technique to measure in situ water vapor, nitrogen and oxygen distribution within the gas channels of an operating PEFC. The use of a gas chromatograph (GC) to measure high levels of water saturation directly, without dehumidification of the flow stream, is a unique aspect of this work. Following careful calibration and instrumentation, a gas chromatograph (GC) was interfaced directly to the fuel cell at various locations along the serpentine anode and cathode flow paths of a specially designed fuel cell. The $50 \, \text{cm}^2$ active area fuel cell also permits simultaneous current distribution measurements via the segmented collector plate approach. The on-line GC method allows discrete measurements of the water vapor content up to a fully saturated condition about every 2 minutes. Water vapor and other species distribution data are shown for several inlet relative humidities on the anode and cathode for different cell voltages. For the thin electrolyte membranes used ($51 \, \mu\text{m}$), there is little functional dependence of the anode gas channel water distribution on current output. For thin membranes, this indicates that there is little gradient in the water activity between anode and cathode, indicating diffusion can offset electro-osmotic drag under these circumstances ($i < 0.5 \, \text{A/cm}^2$). This technique can be used for detailed studies on water distribution and transport in the PEFC.
© 2003 Elsevier B.V. All rights reserved.

Keywords: Mass distribution; Water distribution; PEFC; Flooding; Solid polymer electrolyte

1. Introduction

The hydrogen polymer electrolyte fuel cell (PEFC) has tremendous promise as a future power system due to its low pollution, high efficiency, and stealth. Many studies, too numerous to completely list, have examined various aspects of PEFC performance as a function of operating conditions (e.g. [1–9]). Gottesfeld has written an excellent review of PEFC components and operation, and the reader is referred to it for additional information on PEFC fundamentals [10]. In addition to experimental characterization, much research has been focused on first-principles-based modeling of the PEFC system (e.g. [11–21]). However, advances in modeling of the PEFC have thus far outpaced the ability to experimentally verify the predicted performance. In particular, scant experimental data are presently available regarding current density and species distributions. As indicated by Wang [22], it is this type of detailed val-

idation that will permit an ultimate understanding of the physicochemical phenomena in the PEFC as well as development of useful computer-aided tools for design and development.

Determination of the mass distribution is critical to understanding water management and reactant distribution effects. In particular, it is desirable to understand the water vapor distribution within the gas channels of the flowfield. Many authors have conducted detailed studies or deduced models that describe the water transport through fuel cell components including the electrolyte and porous gas diffusion layers [23–30]. In order to integrate these models and validate their accuracy, it is desired to determine the in situ mole fraction distribution of water vapor, at various locations within the gas channel flow path. A few authors have completed overall water balanced studies in an operating cell by collection of the fuel cell effluent, and condensation of the gas-phase water vapor [31–34]. While insightful, these studies do not provide data on the water distribution throughout the cell, which could vary widely depending on operating conditions, current distribution, and local non-isotropic transport parameters. In order to delineate the effects of

---

* Corresponding author. Tel.: +1-814-865-2519; fax: +1-814-863-4848.
E-mail address: mmm124@psu.edu (M.M. Mench).

current distribution on water distribution, it is also desirable to couple water and current distribution measurements to provide detailed information on non-uniform transport and generation effects. The instrumented cell used in this study allows for simultaneous measurement of current and mass distributions.

Several authors have developed different methodologies for current density distribution [35–39]. The instrumented cell utilized in this work utilizes gold plated, segmented current collector similar to that described by Mench and Wang [40,41]. The reader is referred to these papers for more detail on this methodology for current distribution measurements using a non-segmented MEA. This paper is concerned solely with mass distribution measurement technique.

2. Experimental

2.1. Instrumented cell design

Specific details and geometry of the instrumented fuel cell with segmented flowfield are given in Finckh [42]. The flowfield of the anode and cathode is a single-pass serpentine design. Fig. 1 is a schematic diagram detailing the relevant dimensions of the fuel cell. The dimension of the flow channel was chosen to be 2.2 mm wide,

3.2 mm in depth, and has an average pass length of approximately 71 mm. With a total of 22 serpentine passes, the total path length is 1577 mm. Teflon® gaskets were press fit over the protruding gold-plated rib landings to form a flush surface with the polycarbonate slab. Two additional incompressible sealing gaskets surrounded both gas diffusion layers (GDL) of the MEA to compensate for 70–80% of the GDL thickness. Gold plating, and use of an optimized compression torque for the cell of 35 in. lb minimized electrical contact resistance between rib landings and the GDL. Pressure indicating film (Pressurex® by Sensor Products, Inc.) was used to determine the in situ pressure distribution of the landings onto the MEA, as a function of compression torque. The assembly was checked to ensure a homogeneous pressure distribution from all landings onto the GDL, thus ensuring a uniform contact resistance distribution between the gold-plated landings and GDL. The entire fuel cell assembly was leak-proof tested to 0.3 MPa under water.

A schematic of the test and control system is shown in Fig. 2. Ultra-high purity (>99.999%) hydrogen and standard dry air were supplied from compressed gas-cylinders. A steam-injection humidifier system (Lynntech, Inc.) was used to provide the desired humidification to anode and cathode flows through control of the precise amount of water vapor added to the gas streams. Between humidifier and fuel cell, electric heating tapes were wrapped around the flow lines
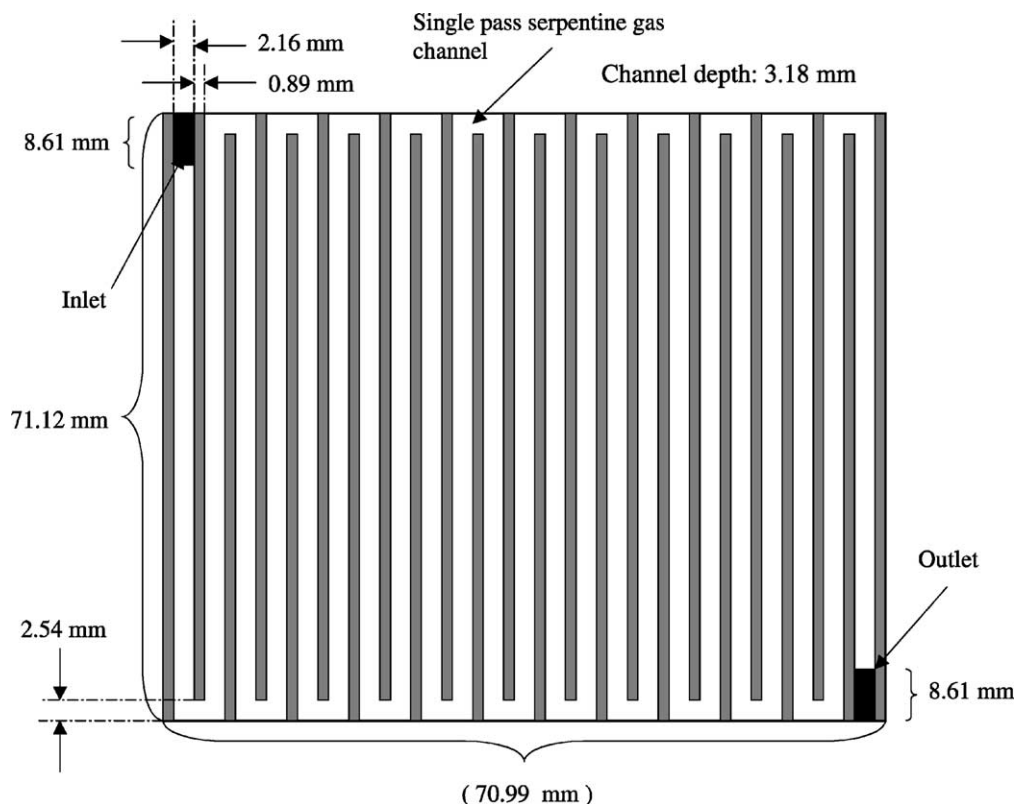

Fig. 1. Schematic diagram of the 50 cm^2 instrumented test cell showing relevant dimensions.
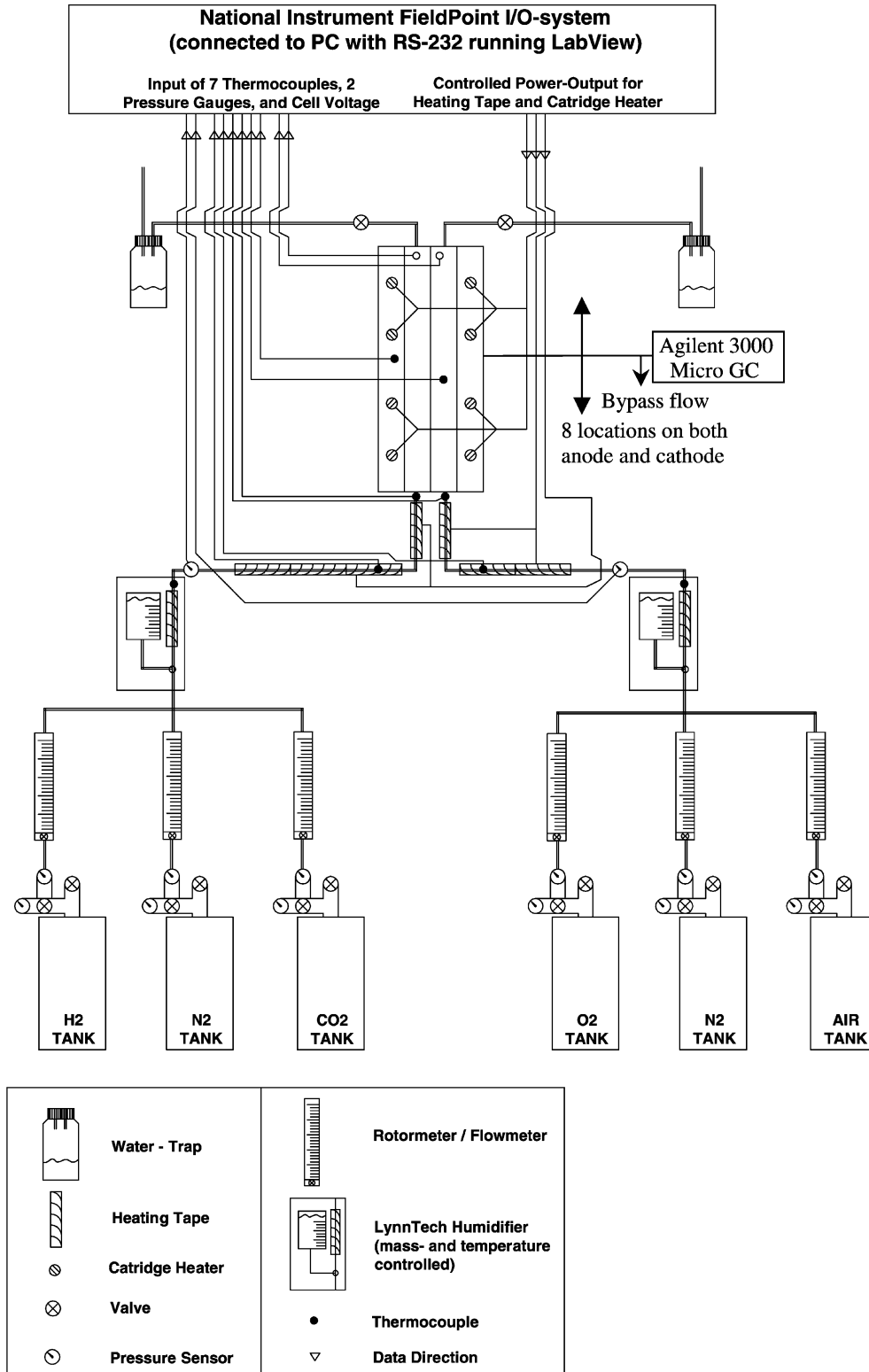
Fig. 2. Schematic of the experimental test stand and control system.

to prevent condensation and maintain desired humidification levels. Directly upstream of the inlet to the fuel cell, a gas sampling port was installed to measure the input humidity to the fuel cell by an Agilent 3000 MicroGC Gas portable chromatograph system. This sampling port was in addition to those along the fuel cell anode and cathode flow paths to provide accurate measurement and control of the humidification entering the cell.

The fuel cell system, including all lines leading to the fuel cell, were heated to the desired temperature, which was maintained with several Omega Engineering, Inc. model 8500 PID controllers. The cell and input lines maintained a steady temperature after suitable time to eliminate thermal transients. This start-up time was determined to be about 90 minutes by system check-out tests using thermocouples affixed to the GDL under non-flowing conditions.

To control and measure accurate current/voltage polarization curves, the fuel cell was connected to a multi-channel potentiostat/galvanostat (Arbin Instruments). For current density measurements, a gold-plated, electrically segmented current collector is used in direct contact with the unaltered GDL on the anode and cathode. In this segmented current collector technique, the potentiostat system maintains a constant voltage and the current sensors measure amperage emerging from each segmented current collector location, without the need for shunt resistors, as described by Mench and Wang [40,41].

The membrane electrode assemblies (MEA) used for testing consisted of Nafion^{TM} 112 as the polymeric membrane, sandwiched between the catalyst and single-sided ELAT^{TM} (E-TEK, Inc.) gas diffusion layers. All MEAs used had a carbon-supported catalyst loading of 0.5 mg Pt/cm^2 on both anode and cathode. Other general operating conditions are given in Table 1.

For mass distribution measurements, eight species extraction ports are located along the anode and cathode serpentine paths of the specialized fuel cell. They are positioned within the 1st, 4th, 7th, 10th, 13th, 16th, 19th, and 22nd reactant channel passes at 4.3, 17.4, 30.4, 43.5, 56.5, 69.6, 82.6, and 95.7% of the fractional distance along the single serpentine path from the channel inlet, respectively. To reduce water droplet blockage and false readings, the extraction takes place along the back wall of the polycarbonate plate, at the farthest distance from the MEA. The fittings on the backing plates used for species extraction were Teflon^{TM} to eliminate galvanic corrosion between various components.

Table 1
Baseline operating conditions

Parameter	Value	Units
Electrolyte	Nafion 112 (E.I. du Pont de Nemours and Company)	NA
Gas diffusion layer	ELAT® (E-TEK of De Nora North America) anode and cathode	NA
Catalyst loading (carbon supported)	0.5	mg/cm^2
Cell temperature	80	°C
Anode inlet temperature	90	°C
Cathode inlet temperature	80	°C
Anode gas	Ultra high purity H$_2$ (>99.999%)	NA
Cathode gas	Commercial air (79% N$_2$, 21% O$_2$)	NA

3. Results and discussion

3.1. Micro GC calibration and measurement

In order to accurately measure the hydrogen, oxygen, nitrogen, and water species present in the fuel cell, an Agilent 3000 MicroGC gas chromatograph (GC) was utilized (Agilent Technologies). For gas species separation, a Plot-U and a molecular sieve (molsieve) GC column was used. The molsieve column was installed with a backflush module for prevention of excess water damage. This type of GC is capable of performing a single measurement about every 2 minutes. The column temperature was set to 120 °C to avoid internal water condensation, and carrier gases of UHP helium, a 7.5% H$_2$ balance helium, or argon were used. The GC was interfaced to the fuel cell through a 0.32 cm (0.125 in.) stainless steel, heated tube connected to the sample ports of the cell. The sample line temperature from fuel cell to the GC was monitored and kept well above 100 °C. Since low-pressure gas flow can hold a greater mole fraction of water than higher-pressure gas flow, there is no condensation resulting from the pressure drop from the fuel cell channel to the GC inlet. The flow is directed toward a bypass valve that allows continuous flow of atmospheric pressure sample gas from the fuel cell and past the GC sample inlet. Sample availability at atmospheric pressure eliminates error associated with varying sample inlet pressure, which can greatly affect results. The bypass flow was measured continuously with a mass flow meter to ensure that the extracted sample was a small fraction of the total fuel cell reactant flow. Typical values of bypass were 2–3% of the total flow, and this value never exceeded 5% during measurement. The possible disruption of performance by sample extraction was examined and determined to be minimal. Fig. 3 shows continuous performance measurements between cell conditions of 0.4, 0.6, and 0.8 V while sample extraction was occurring at many locations along the anode path. During this continuous measurement, the sample extraction line was removed and replaced at several different locations, and many samples were taken. It is clear from this figure that no significant performance change results from withdrawal of such a small fraction of total flow from the channel. In addition, the reproducibility of the current distribution results over long time scales and through voltage cycling is demonstrated with Fig. 3.

Depending on the pressure of the fuel cell, the delivery time for species from the fuel cell to the GC varied from seconds to minutes, based on calculations of interior tube volume and known flow rate. All GC measurements were given adequate time to ensure ample tube purge had occurred, and several measurements were taken to ensure repeatability of the measurement.

In typical GC measurement applications, water vapor is condensed from the flow before entering the GC device. This is to prevent damage or degradation to the columns and detector elements. Indeed, if liquid water reaches the inlet
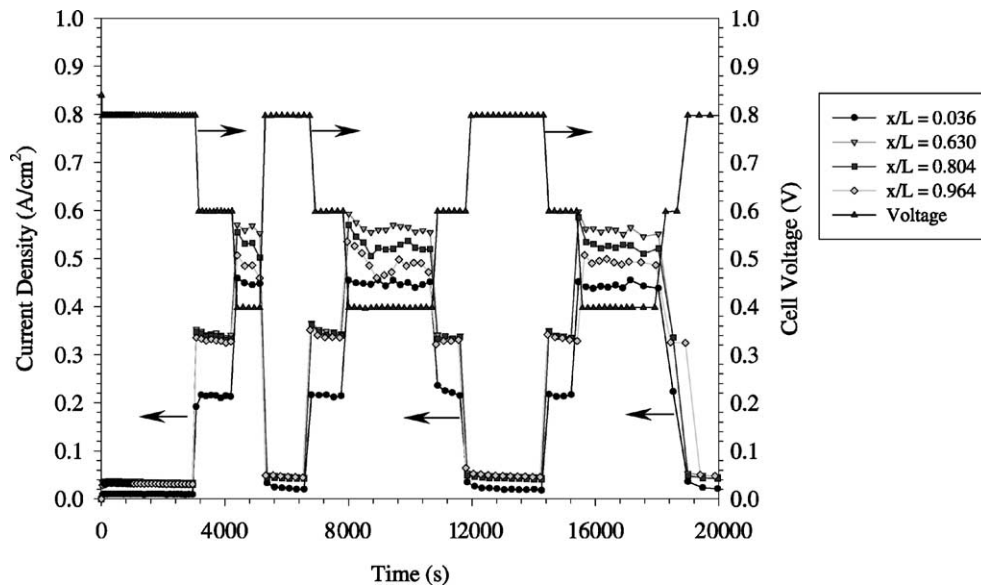
Fig. 3. Time varying performance at 0.4, 0.6, and 0.8 V while mass distribution measurements were taken along anode path, indicating little effect of measurement on cell performance.

of the GC or condenses inside the detector, system failure will likely occur. However, all temperatures of the columns, inlets, and sample tubes are kept well above 100 °C to prevent this. Because of the high amount of water present at elevated temperature and resultant accelerated deactivation of the separation columns, a backflush module was installed to block vapor flow into the molsieve column, and frequent GC column bakeout was conducted. Provided that all flow is maintained well above the dew point, very accurate and repeatable measurement of water content up to 90 mole% fraction can be achieved.

3.1.1. Sample calibration

Calibration is required before every set of experiments to maintain accuracy of measurement. Calibration is accomplished with a gas-bubbler humidifier at very low flow rate and controlled temperature as a standard to ensure a known exit humidity of the calibration gas mixture. The gas leaving the humidifier is precisely monitored. Pressure must also be monitored at the humidifier exit to correct for any losses from the humidifier exit to the GC sample inlet. A single point calibration is made at a low humidifier exit temperature of around 50 °C, to correlate the measured response area to the thermodynamically known water vapor mole fraction. Then, the temperature of the humidifier is increased and the calibration correlation coefficient is not altered, but the output is checked against the theoretical value to ensure accuracy. The results are very consistent. The measured mole fraction is typically within ±2% of the theoretical value, up to very high values of water mole fraction up to 95 °C. Calibration curves taken for fully humidified hydrogen and fully humidified airflow are shown in Figs. 4 and 5. The data shown represent an average of five measurements with very little scat-

ter, and it can be seen that the expected accuracy is around ±2%. Note the close agreement between the measured values of water fraction compared to the thermodynamically expected values, which change very steeply with temperature in the range of fuel cell operation. This calibration also indicates that the precisely temperature and pressure controlled humidifier is near 100% efficiency at these extremely low flow rate conditions. Due to the steepness of the theoretical water vapor mole fraction curve, if the humidifier were significantly less than 100% efficient, the measured calibration curve would not follow the rapidly changing slope of
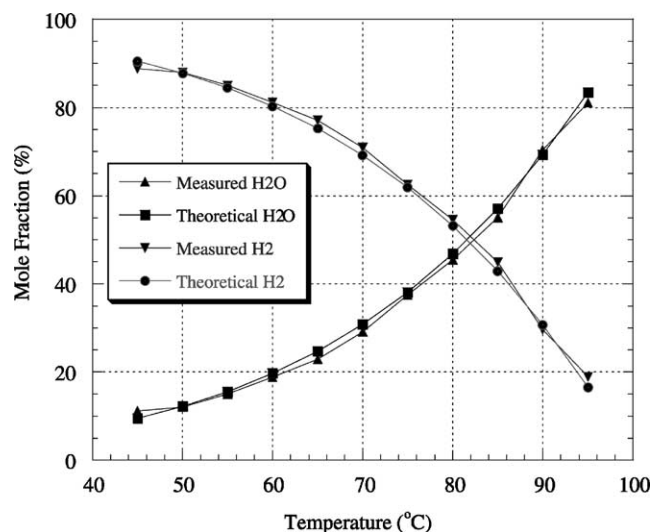

Fig. 4. Comparison between measured and theoretical water vapor and hydrogen concentrations measured with GC with baseline value at 50 °C. The humidifier bottle was at 1.1 atm pressure.
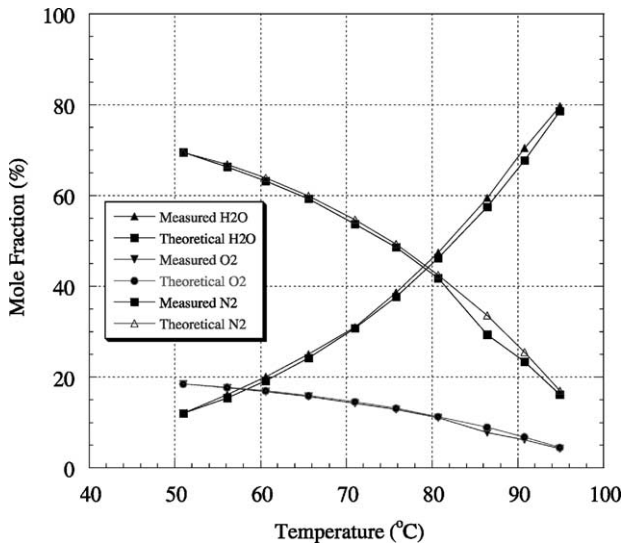
Fig. 5. Comparison between measured and theoretical water vapor, nitrogen and oxygen concentrations measured with GC with baseline value at 50 °C. The humidifier bottle was at 1.1 atm pressure.

the theoretical curve. Calibration with increased flow rates will lead to departure from the theoretical curve as shown in Figs. 4 and 5, indicating that the humidifier is less than 100% efficient as flow rate is increased.

3.1.2. Anode water concentration distribution

Fig. 6 shows the measured water mole fraction at various locations within the anode flow channel for three fuel cell voltages. The current distribution associated with these measurements is shown in Fig. 3. The fuel cell exit pressure was ambient, with 100% humidification at 80 °C on the air cathode, and either 100 or 0% RH at 65 °C on the anode. Each data point shown represents an average of at least five data points. There was very little scatter in the data. This series of tests were designed to illustrate the following:

1. The uptake of water into the gas channel from dry inlet conditions in the anode.
2. The effect of current density (and thus changing electro-osmotic drag of water through the PEFC) on anode gas channel humidity ratio.

It can be seen from Fig. 6, that for both the cases of different inlet humidity ratio, the water uptake follows an exponential approach to an asymptotic value that is greater than the thermodynamically allowed maximum at the cell temperature of 80 °C. One explanation for increased water content is that the cell temperature should be higher than the prescribed 80 °C, due to heat generation from electrochemical reaction and resistive dissipation. In addition, it should be noted that the inlet gas temperature to the anode was 90 °C, while the cell temperature was maintained at 80 °C. A one-degree temperature difference would account for a 5% change in the maximum theoretical mole fraction, within the limits of measurement.

It can also be seen from Fig. 6, that in most cases, the measured anode channel water content was not affected to a great degree by the voltage (and hence current) draw. In
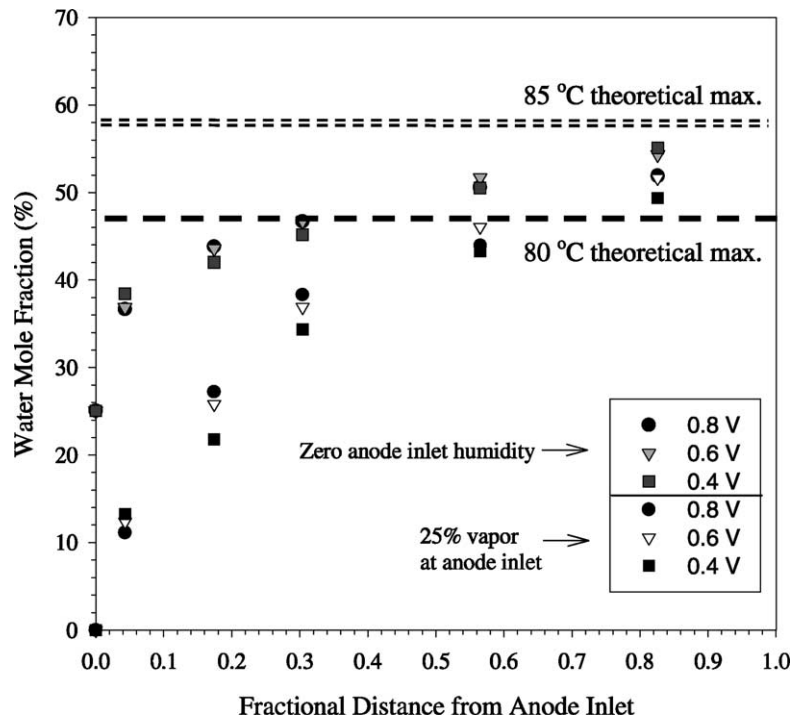

Fig. 6. Measured water distribution as a function of fractional distance from anode inlet for partially, and non-humidified anode conditions. Test conditions: exit pressure A/C = 1 atm, 100% RH @ 80 °C air cathode, 100 or 0% RH @ 65 °C neat H_2 anode, ξ_c: 1.75 A/cm^2 equivalent, ξ_a: 0.7 A/cm^2 equivalent.
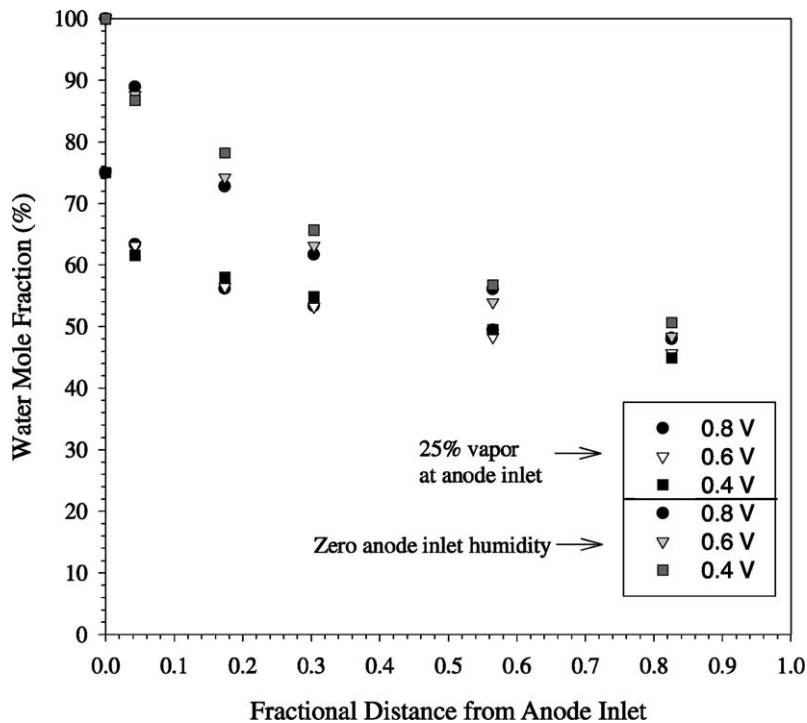
Fig. 7. Deduced hydrogen distribution as a function of fractional distance from anode inlet for partially, and non-humidified cathode conditions. Test conditions: exit pressure A/C = 1 atm, 100% RH @ 80 °C air cathode, 100 or 0% RH @ 65 °C neat H_2 anode ξ_c: 1.75 A/cm^2 equivalent, ξ_a: 0.7 A/cm^2 equivalent.

most cases, the highest current output (lowest cell voltage) condition resulted in the lowest measured anode channel water vapor content, although not to a very significant degree. This strongly indicates that the electro-osmotic drag of water from the anode to the cathode is nearly evenly balanced by back diffusion under these conditions ($i < 0.5$ A/cm^2). This is expected for very thin membranes, such as the 51 μm Nafion PEFC used for testing. This near balance of drag and diffusion of water with thin membranes has been observed experimentally by water condensation and collection techniques as well [32].

Fig. 7 shows the deduced hydrogen mole fraction variation along the anode flow path for the test conditions shown in Fig. 6. Here, the fact that hydrogen is the only other species present in the anode was used to deduce the hydrogen mole fraction. Because the anode gas channel showed a tendency to uptake water more slowly for low cell voltage (corresponding to higher electro-osmotic drag), the deduced hydrogen mole fraction in the anode shows a slightly inverse relationship between cell voltage and mole fraction, despite the fact consumption is higher for low cell voltages. It should be noted that this variation, while systematic, is believed to be within the error of measurement estimated to be between 2 and 5 mole% fraction.

3.1.3. Cathode water concentration distribution

Fig. 8 shows the measured water mole fraction at various locations within the cathode flow channel for three fuel cell voltages. There was 100% humidification at 90 °C on the

anode, and either 0 or 20% water vapor mole fraction at the air cathode inlet. Each data point shown represents an average of at least five data points with scatter less than ±2.5 mole% fraction in the data. This series of tests were designed to illustrate the uptake of water into the gas channel from dry inlet conditions in the cathode.

It can be seen from Fig. 8 that the two cathode inlet humidity cases had different water vapor uptake results. For the case of an inlet relative humidity of 20%, cell performance was sufficient to provide adequate water generation at the cathode to ensure a saturated flow condition at the exit. However, for the 0% relative humidity inlet condition, there was very low cell performance. The maximum cell average current density for the conditions shown was only 0.4 A/cm^2. Therefore, water uptake was not complete to saturation. It can be seen from these plots that water generation at the cathode does have a strong affect on cathode gas channel water uptake for these conditions, as both measured curves show increased uptake for lower cell voltage corresponding to increased generation and electro-osmotic drag. Since the anode uptake was not affected to a great degree by changes in current output, indicating electro-osmotic drag to the cathode was nearly compensated by diffusion of water to the anode, it seems that the water uptake in the cathode gas channel is mostly the water produced via water generation for this set of test conditions.

Figs. 9 and 10 show the measured nitrogen and oxygen mole fractions in the cathode flow path for the two cases of different cathode inlet humidity shown in Fig. 8. Because
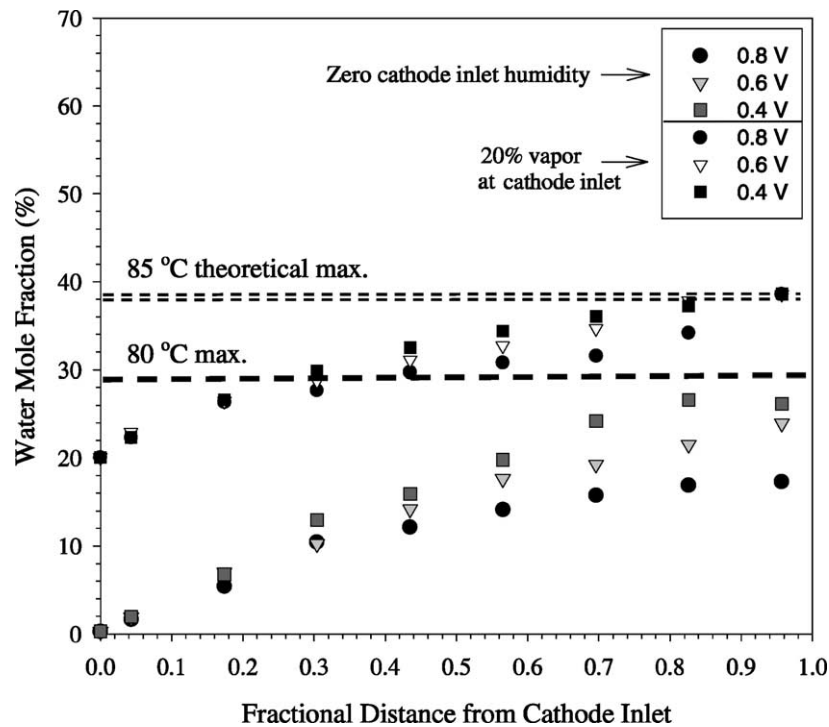
Fig. 8. Measured water vapor distribution as a function of fractional distance from cathode inlet for partially, and non-humidified cathode conditions. Test conditions: exit pressure A/C = 1.5 atm, 100% RH @ 90 °C hydrogen anode, 100 or 0% RH @ 65 °C neat H_2 anode, ξ_c: 2.0 A/cm^2 equivalent, ξ_a: 1.5 A/cm^2 equivalent.

of the high true stoichiometry, the changes in oxygen mole fraction are low, around 7%. It should be noted that the stoichiometry values reported are for an equivalent total current density. That is, the flow rate is constant for each cell volt-

age, regardless of the resultant cell current output. This is required with the segmented cell approach, as each location will have a different output and it is thus extremely difficult to match the flow rate with the measured bulk current
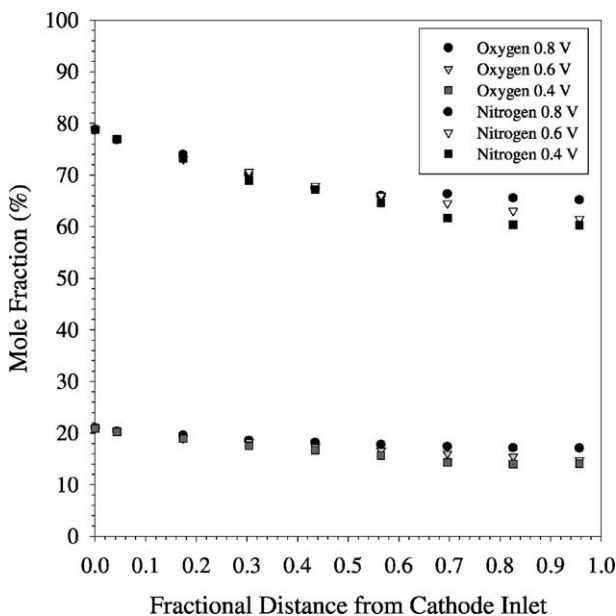

Fig. 9. Measured oxygen and nitrogen distribution as a function of fractional distance from cathode inlet for non-humidified cathode conditions. Test conditions: exit pressure A/C = 1.5 atm, 100% RH @ 90 °C hydrogen anode, 0% RH air cathode, ξ_c: 2.0 A/cm^2 equivalent. ξ_a: 1.5 A/cm^2 equivalent.
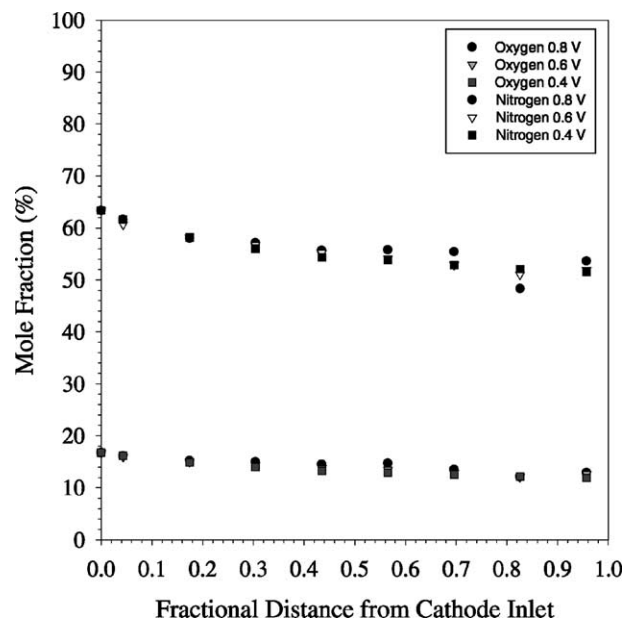

Fig. 10. Measured oxygen and nitrogen distribution as a function of fractional distance from cathode inlet for under humidified cathode conditions. Test conditions: exit pressure A/C = 1.5 atm, 100% RH @ 90 °C hydrogen anode, 20 mole% fraction inlet air cathode, ξ_c: 2.0 A/cm^2 equivalent, ξ_a: 1.5 A/cm^2 equivalent.

density. Values of both Figs. 9 and 10 are within 5% of the expected theoretical value based on current output and flow rate.

4. Conclusions

Gas chromatography has been used to measure the in situ flow channel water vapor distribution with full humidification in an operating fuel cell flow field. This technique can be used to directly map water distribution in the anode and cathode of an operating fuel cell with a time resolution of approximately 2 minutes, and a spatial resolution limited only by the proximity of sample extraction ports located in the reactant gas channels. Along with other diagnostic techniques such as current distribution mapping, this species mapping technique provides an important tool to understand water management and reactant distribution in PEFC. The anode channel water distribution was not greatly influenced by the current density, while the cathode water uptake showed some dependence on current density, especially at low overall cell performance. For the thin (51 μm) membranes used, the electro-osmotic drag of water from the anode to the cathode is nearly evenly balanced by back diffusion under low to medium performance conditions ($i < 0.5\,\text{A/cm}^2$). This new diagnostic technique enables future work that will address in detail the coupling of current and water distribution.

Acknowledgements

References

[1] A. Parthasarathy, S. Srinivasan, A.J. Appleby, C. Martin, J. Electrochem. Soc. 139 (1992) 2530.
[2] A. Parthasarathy, S. Srinivasan, A.J. Appleby, C. Martin, J. Electrochem. Soc. 139 (1992) 2856.
[3] Y.W. Rho, O.A. Velev, S. Srinivasan, Y.T. Kho, J. Electrochem. Soc. 141 (1994) 3838.
[4] J.C. Amphlett, R.M. Baumert, R.F. Mann, B.A. Peppley, P.R. Roberge, T.J. Harris, J. Electrochem. Soc. 142 (1995) 9.
[5] R. Mosdale, S. Srinivasan, Electrochim. Acta 40 (1995) 413.
[6] H.-F. Oetjen, V.M. Schmidt, U. Stimming, F. Trila, J. Electrochem. Soc. 143 (1996) 3838.
[7] F.N. Büchi, D. Srinivasan, J. Electrochem. Soc. 144 (1997) 2767.
[8] F.A. Uribe, S. Gottesfeld, T.A. Zawodzinski, J. Electrochem. Soc. 149 (2002) A293.
[9] E.A. Ticianelli, C.R. Derouin, S. Srinivasan, J. Electroanal. Chem. 251 (1988) 275.
[10] S. Gottesfeld, in: C. Tobias (Ed.), Advances in Electrochemical Science and Engineering, vol. 5, Wiley, New York, 1997.
[11] T.E. Springer, T.A. Zawodinski, S. Gottesfeld, J. Electrochem. Soc. 138 (1991) 2334.
[12] D.M. Bernardi, M.W. Verbrugge, AIChE J. 37 (1991) 1151.
[13] D.M. Bernardi, M.W. Verbrugge, J. Electrochem. Soc. 139 (1992) 2477.
[14] T.E. Springer, M.S. Wilson, S. Gottesfeld, J. Electrochem. Soc. 140 (1993) 3513.
[15] T.V. Nguyen, R.E. White, J. Electrochem. Soc. 140 (1993) 2178.
[16] C.Y. Wang, W.B. Gu, J. Electrochem. Soc. 145 (1998) 3407.
[17] V. Gurau, H. Liu, S. Kakac, AIChE J. 44 (1998) 2410.
[18] J.S. Yi, T.V. Nguyen, J. Electrochem. Soc. 146 (1999) 38.
[19] S. Um, C.Y. Wang, K.S. Chen, J. Electrochem. Soc. 147 (2000) 4485.
[20] Z.H. Wang, C.Y. Wang, K.S. Chen, J. Power Sources 94 (2001) 40.
[21] C.Y. Wang, S. Um, H. Meng, U. Pasaogullari, Y. Wang, in: Proceedings of the 2002 Fuel Cell Seminar on Computational Fuel Cell Dynamics (CFCD) Models, November 2002.
[22] C.Y. Wang, Two-phase flow and transport in PEM fuel cells, in: Handbook of Fuel Cells, Wiley, New York, 2002.
[23] D.M. Bernardi, J. Electrochem. Soc. 137 (1990) 3344.
[24] T.E. Springer, T.A. Zawodzinski, S. Gottesfeld, J. Electrochem. Soc. 138 (1991) 2334.
[25] D.M. Bernardi, M.W. Verbrugge, J. Electrochem. Soc. 139 (1992) 2477.
[26] T.F. Fuller, J. Newman, J. Electrochem. Soc. 140 (1993) 1218.
[27] M. Eikerling, Y.I. Kharkats, A.A. Kornyshev, Y.M. Volfkovich, J. Electrochem. Soc. 145 (1999) 2684.
[28] J.S. Yi, T.V. Nguyen, J. Electrochem. Soc. 146 (1999) 38.
[29] I-M. Hsing, P. Futerko, Chem. Eng. Sci. 55 (2000) 4209.
[30] Z.H. Wang, C.Y. Wang, K.S. Chen, J. Power Sources 94 (2001) 40.
[31] X. Ren, S. Gottesfeld, J. Electrochem. Soc. 148 (2001) A87.
[32] G.J. Janssen, J. Electrochem. Soc. 148 (2001) A1313.
[33] G.J. Janssen, M.L. Overvelde, J. Power Sources 101 (2001) 117.
[34] W.K. Lee, J.W. Van Zee, S. Shimpalee, S. Dutta, Proc. ASME Heat Transfer Div. 1 (1999) 339.
[35] C. Wieser, A. Helmbold, E. Gülzow, J. Appl. Electrochem. 30 (2000) 803.
[36] J. Stumper, S. Campbell, D. Wilkinson, M. Johnson, M. Davis, Electrochim. Acta 43 (1998) 3773.
[37] S. Cleghorn, C. Derouin, M. Wilson, S. Gottesfeld, J. Appl. Electrochem. 28 (1998) 663.
[38] M. Noponen, T. Mennola, M. Mikkola, T. Hottinen, P. Lund, J. Power Sources 106 (2002) 304.
[39] D. Brett, S. Atkins, N. Brandon, V. Vesovic, N. Vasileiadis, A. Kucernak, Electrochem. Comm. 3 (2001) 628.
[40] M. Mench, C.Y. Wang, J. Electrochem. Soc. 150 (2003) A79.
[41] M. Mench, C.Y. Wang, M. Ishikawa, J. Electrochem. Soc. 150 (2003) A1052.
[42] O.H. Finckh, Dilution effects and current distribution on hydrogen proton exchange membrane fuel cells, MS thesis, The Pennsylvania State University, Pennsylvania, May 2002.